Measurement of Branching Fractions for Two-Body Charmless *B* Decays to Charged Pions and Kaons at *BaBar*

The *BaBar* Collaboration

Measurement of branching fractions for two-body charmless B decays to charged pions and kaons at *BABAR*

The *BABAR* Collaboration

August 21, 2000

Abstract

We present preliminary results of a search for charmless two-body B decays to charged pions and kaons using data collected by the *BABAR* detector at the Stanford Linear Accelerator Center's PEP-II storage ring. In a sample of 8.8 million produced $B\overline{B}$ pairs we measure the branching fractions $\mathcal{B}(B^0 \to \pi^+\pi^-) = (9.3^{+2.6+1.2}_{-2.3-1.4}) \times 10^{-6}$ and $\mathcal{B}(B^0 \to K^+\pi^-) = (12.5^{+3.0+1.3}_{-2.6-1.7}) \times 10^{-6}$, where the first uncertainty is statistical and the second is systematic. For the decay $B^0 \to K^+K^-$ we find no significant signal and set an upper limit of $\mathcal{B}(B^0 \to K^+K^-) < 6.6 \times 10^{-6}$ at the 90% confidence level.

The *BABAR* Collaboration

B. Aubert, A. Boucham, D. Boutigny, I. De Bonis, J. Favier, J.-M. Gaillard, F. Galeazzi, A. Jeremie,
Y. Karyotakis, J. P. Lees, P. Robbe, V. Tisserand, K. Zachariadou

Lab de Phys. des Particules, F-74941 Annecy-le-Vieux, CEDEX, France

A. Palano

Università di Bari, Dipartimento di Fisica and INFN, I-70126 Bari, Italy

G. P. Chen, J. C. Chen, N. D. Qi, G. Rong, P. Wang, Y. S. Zhu

Institute of High Energy Physics, Beijing 100039, China

G. Eigen, P. L. Reinertsen, B. Stugu

University of Bergen, Inst. of Physics, N-5007 Bergen, Norway

B. Abbott, G. S. Abrams, A. W. Borgland, A. B. Breon, D. N. Brown, J. Button-Shafer, R. N. Cahn,
A. R. Clark, Q. Fan, M. S. Gill, S. J. Gowdy, Y. Groysman, R. G. Jacobsen, R. W. Kadel, J. Kadyk,
L. T. Kerth, S. Kluth, J. F. Kral, C. Leclerc, M. E. Levi, T. Liu, G. Lynch, A. B. Meyer, M. Momayezi,
P. J. Oddone, A. Perazzo, M. Pripstein, N. A. Roe, A. Romosan, M. T. Ronan, V. G. Shelkov, P. Strother,
A. V. Telnov, W. A. Wenzel

Lawrence Berkeley National Lab, Berkeley, CA 94720, USA

P. G. Bright-Thomas, T. J. Champion, C. M. Hawkes, A. Kirk, S. W. O'Neale, A. T. Watson, N. K. Watson

University of Birmingham, Birmingham, B15 2TT, UK

T. Deppermann, H. Koch, J. Krug, M. Kunze, B. Lewandowski, K. Peters, H. Schmuecker, M. Steinke

Ruhr Universität Bochum, Inst. f. Experimentalphysik 1, D-44780 Bochum, Germany

J. C. Andress, N. Chevalier, P. J. Clark, N. Cottingham, N. De Groot, N. Dyce, B. Foster, A. Mass,
J. D. McFall, D. Wallom, F. F. Wilson

University of Bristol, Bristol BS8 lTL, UK

K. Abe, C. Hearty, T. S. Mattison, J. A. McKenna, D. Thiessen

University of British Columbia, Vancouver, BC, Canada V6T 1Z1

B. Camanzi, A. K. McKemey, J. Tinslay

Brunel University, Uxbridge, Middlesex UB8 3PH, UK

V. E. Blinov, A. D. Bukin, D. A. Bukin, A. R. Buzykaev, M. S. Dubrovin, V. B. Golubev,
V. N. Ivanchenko, A. A. Korol, E. A. Kravchenko, A. P. Onuchin, A. A. Salnikov, S. I. Serednyakov,
Yu. I. Skovpen, A. N. Yushkov

Budker Institute of Nuclear Physics, Siberian Branch of Russian Academy of Science, Novosibirsk 630090,
Russia

A. J. Lankford, M. Mandelkern, D. P. Stoker

University of California at Irvine, Irvine, CA 92697, USA

A. Ahsan, K. Arisaka, C. Buchanan, S. Chun

University of California at Los Angeles, Los Angeles, CA 90024, USA

J. G. Branson, R. Faccini,[1] D. B. MacFarlane, Sh. Rahatlou, G. Raven, V. Sharma

University of California at San Diego, La Jolla, CA 92093, USA

C. Campagnari, B. Dahmes, P. A. Hart, N. Kuznetsova, S. L. Levy, O. Long, A. Lu, J. D. Richman,
W. Verkerke, M. Witherell, S. Yellin

University of California at Santa Barbara, Santa Barbara, CA 93106, USA

J. Beringer, D. E. Dorfan, A. Eisner, A. Frey, A. A. Grillo, M. Grothe, C. A. Heusch, R. P. Johnson,
W. Kroeger, W. S. Lockman, T. Pulliam, H. Sadrozinski, T. Schalk, R. E. Schmitz, B. A. Schumm,
A. Seiden, M. Turri, D. C. Williams

University of California at Santa Cruz, Institute for Particle Physics, Santa Cruz, CA 95064, USA

E. Chen, G. P. Dubois-Felsmann, A. Dvoretskii, D. G. Hitlin, Yu. G. Kolomensky, S. Metzler, J. Oyang,
F. C. Porter, A. Ryd, A. Samuel, M. Weaver, S. Yang, R. Y. Zhu

California Institute of Technology, Pasadena, CA 91125, USA

R. Aleksan, G. De Domenico, A. de Lesquen, S. Emery, A. Gaidot, S. F. Ganzhur, G. Hamel de
Monchenault, W. Kozanecki, M. Langer, G. W. London, B. Mayer, B. Serfass, G. Vasseur, C. Yeche,
M. Zito

Centre d'Etudes Nucléaires, Saclay, F-91191 Gif-sur-Yvette, France

S. Devmal, T. L. Geld, S. Jayatilleke, S. M. Jayatilleke, G. Mancinelli, B. T. Meadows, M. D. Sokoloff

University of Cincinnati, Cincinnati, OH 45221, USA

J. Blouw, J. L. Harton, M. Krishnamurthy, A. Soffer, W. H. Toki, R. J. Wilson, J. Zhang

Colorado State University, Fort Collins, CO 80523, USA

S. Fahey, W. T. Ford, F. Gaede, D. R. Johnson, A. K. Michael, U. Nauenberg, A. Olivas, H. Park,
P. Rankin, J. Roy, S. Sen, J. G. Smith, D. L. Wagner

University of Colorado, Boulder, CO 80309, USA

T. Brandt, J. Brose, G. Dahlinger, M. Dickopp, R. S. Dubitzky, M. L. Kocian, R. Müller-Pfefferkorn,
K. R. Schubert, R. Schwierz, B. Spaan, L. Wilden

Technische Universität Dresden, Inst. f. Kern- u. Teilchenphysik, D-01062 Dresden, Germany

L. Behr, D. Bernard, G. R. Bonneaud, F. Brochard, J. Cohen-Tanugi, S. Ferrag, E. Roussot, C. Thiebaux,
G. Vasileiadis, M. Verderi

Ecole Polytechnique, Lab de Physique Nucléaire H. E., F-91128 Palaiseau, France

A. Anjomshoaa, R. Bernet, F. Di Lodovico, F. Muheim, S. Playfer, J. E. Swain

University of Edinburgh, Edinburgh EH9 3JZ, UK

C. Bozzi, S. Dittongo, M. Folegani, L. Piemontese

Università di Ferrara, Dipartimento di Fisica and INFN, I-44100 Ferrara, Italy

E. Treadwell

Florida A&M University, Tallahassee, FL 32307, USA

---

[1]Jointly appointed with Università di Roma La Sapienza, Dipartimento di Fisica and INFN, I-00185 Roma, Italy

3

R. Baldini-Ferroli, A. Calcaterra, R. de Sangro, D. Falciai, G. Finocchiaro, P. Patteri, I. M. Peruzzi,[2]
M. Piccolo, A. Zallo

Laboratori Nazionali di Frascati dell'INFN, I-00044 Frascati, Italy

S. Bagnasco, A. Buzzo, R. Contri, G. Crosetti, P. Fabbricatore, S. Farinon, M. Lo Vetere, M. Macri,
M. R. Monge, R. Musenich, R. Parodi, S. Passaggio, F. C. Pastore, C. Patrignani, M. G. Pia, C. Priano,
E. Robutti, A. Santroni

Università di Genova, Dipartimento di Fisica and INFN, I-16146 Genova, Italy

J. Cochran, H. B. Crawley, P.-A. Fischer, J. Lamsa, W. T. Meyer, E. I. Rosenberg

Iowa State University, Ames, IA 50011-3160, USA

R. Bartoldus, T. Dignan, R. Hamilton, U. Mallik

University of Iowa, Iowa City, IA 52242, USA

C. Angelini, G. Batignani, S. Bettarini, M. Bondioli, M. Carpinelli, F. Forti, M. A. Giorgi, A. Lusiani,
M. Morganti, E. Paoloni, M. Rama, G. Rizzo, F. Sandrelli, G. Simi, G. Triggiani

Università di Pisa, Scuola Normale Superiore, and INFN, I-56010 Pisa, Italy

M. Benkebil, G. Grosdidier, C. Hast, A. Hoecker, V. LePeltier, A. M. Lutz, S. Plaszczynski, M. H. Schune,
S. Trincaz-Duvoid, A. Valassi, G. Wormser

LAL, F-91898 ORSAY Cedex, France

R. M. Bionta, V. Brigljević, O. Fackler, D. Fujino, D. J. Lange, M. Mugge, X. Shi, T. J. Wenaus,
D. M. Wright, C. R. Wuest

Lawrence Livermore National Laboratory, Livermore, CA 94550, USA

M. Carroll, J. R. Fry, E. Gabathuler, R. Gamet, M. George, M. Kay, S. McMahon, T. R. McMahon,
D. J. Payne, C. Touramanis

University of Liverpool, Liverpool L69 3BX, UK

M. L. Aspinwall, P. D. Dauncey, I. Eschrich, N. J. W. Gunawardane, R. Martin, J. A. Nash, P. Sanders,
D. Smith

University of London, Imperial College, London, SW7 2BW, UK

D. E. Azzopardi, J. J. Back, P. Dixon, P. F. Harrison, P. B. Vidal, M. I. Williams

University of London, Queen Mary and Westfield College, London, E1 4NS, UK

G. Cowan, M. G. Green, A. Kurup, P. McGrath, I. Scott

University of London, Royal Holloway and Bedford New College, Egham, Surrey TW20 0EX, UK

D. Brown, C. L. Davis, Y. Li, J. Pavlovich, A. Trunov

University of Louisville, Louisville, KY 40292, USA

J. Allison, R. J. Barlow, J. T. Boyd, J. Fullwood, A. Khan, G. D. Lafferty, N. Savvas, E. T. Simopoulos,
R. J. Thompson, J. H. Weatherall

University of Manchester, Manchester M13 9PL, UK

---

[2]Jointly appointed with Univ. di Perugia, I-06100 Perugia, Italy

C. Dallapiccola, A. Farbin, A. Jawahery, V. Lillard, J. Olsen, D. A. Roberts

University of Maryland, College Park, MD 20742, USA

B. Brau, R. Cowan, F. Taylor, R. K. Yamamoto

Massachusetts Institute of Technology, Lab for Nuclear Science, Cambridge, MA 02139, USA

G. Blaylock, K. T. Flood, S. S. Hertzbach, R. Kofler, C. S. Lin, S. Willocq, J. Wittlin

University of Massachusetts, Amherst, MA 01003, USA

P. Bloom, D. I. Britton, M. Milek, P. M. Patel, J. Trischuk

McGill University, Montreal, PQ, Canada H3A 2T8

F. Lanni, F. Palombo

Università di Milano, Dipartimento di Fisica and INFN, I-20133 Milano, Italy

J. M. Bauer, M. Booke, L. Cremaldi, R. Kroeger, J. Reidy, D. Sanders, D. J. Summers

University of Mississippi, University, MS 38677, USA

J. F. Arguin, J. P. Martin, J. Y. Nief, R. Seitz, P. Taras, A. Woch, V. Zacek

Université de Montreal, Lab. Rene J. A. Levesque, Montreal, QC, Canada, H3C 3J7

H. Nicholson, C. S. Sutton

Mount Holyoke College, South Hadley, MA 01075, USA

N. Cavallo, G. De Nardo, F. Fabozzi, C. Gatto, L. Lista, D. Piccolo, C. Sciacca

Università di Napoli Federico II, Dipartimento di Scienze Fisiche and INFN, I-80126 Napoli, Italy

M. Falbo

Northern Kentucky University, Highland Heights, KY 41076, USA

J. M. LoSecco

University of Notre Dame, Notre Dame, IN 46556, USA

J. R. G. Alsmiller, T. A. Gabriel, T. Handler

Oak Ridge National Laboratory, Oak Ridge, TN 37831, USA

F. Colecchia, F. Dal Corso, G. Michelon, M. Morandin, M. Posocco, R. Stroili, E. Torassa, C. Voci

Università di Padova, Dipartimento di Fisica and INFN, I-35131 Padova, Italy

M. Benayoun, H. Briand, J. Chauveau, P. David, C. De la Vaissière, L. Del Buono, O. Hamon, F. Le Diberder, Ph. Leruste, J. Lory, F. Martinez-Vidal, L. Roos, J. Stark, S. Versillé

Universités Paris VI et VII, Lab de Physique Nucléaire H. E., F-75252 Paris, Cedex 05, France

P. F. Manfredi, V. Re, V. Speziali

Università di Pavia, Dipartimento di Elettronica and INFN, I-27100 Pavia, Italy

E. D. Frank, L. Gladney, Q. H. Guo, J. H. Panetta

University of Pennsylvania, Philadelphia, PA 19104, USA

M. Haire, D. Judd, K. Paick, L. Turnbull, D. E. Wagoner

Prairie View A&M University, Prairie View, TX 77446, USA

5

J. Albert, C. Bula, M. H. Kelsey, C. Lu, K. T. McDonald, V. Miftakov, S. F. Schaffner, A. J. S. Smith,
A. Tumanov, E. W. Varnes

Princeton University, Princeton, NJ 08544, USA

G. Cavoto, F. Ferrarotto, F. Ferroni, K. Fratini, E. Lamanna, E. Leonardi, M. A. Mazzoni, S. Morganti,
G. Piredda, F. Safai Tehrani, M. Serra

Università di Roma La Sapienza, Dipartimento di Fisica and INFN, I-00185 Roma, Italy

R. Waldi

Universität Rostock, D-18051 Rostock, Germany

P. F. Jacques, M. Kalelkar, R. J. Plano

Rutgers University, New Brunswick, NJ 08903, USA

T. Adye, U. Egede, B. Franek, N. I. Geddes, G. P. Gopal

Rutherford Appleton Laboratory, Chilton, Didcot, Oxon., OX11 0QX, UK

N. Copty, M. V. Purohit, F. X. Yumiceva

University of South Carolina, Columbia, SC 29208, USA

I. Adam, P. L. Anthony, F. Anulli, D. Aston, K. Baird, E. Bloom, A. M. Boyarski, F. Bulos, G. Calderini,
M. R. Convery, D. P. Coupal, D. H. Coward, J. Dorfan, M. Doser, W. Dunwoodie, T. Glanzman,
G. L. Godfrey, P. Grosso, J. L. Hewett, T. Himel, M. E. Huffer, W. R. Innes, C. P. Jessop, P. Kim,
U. Langenegger, D. W. G. S. Leith, S. Luitz, V. Luth, H. L. Lynch, G. Manzin, H. Marsiske, S. Menke,
R. Messner, K. C. Moffeit, M. Morii, R. Mount, D. R. Muller, C. P. O'Grady, P. Paolucci, S. Petrak,
H. Quinn, B. N. Ratcliff, S. H. Robertson, L. S. Rochester, A. Roodman, T. Schietinger, R. H. Schindler,
J. Schwiening, G. Sciolla, V. V. Serbo, A. Snyder, A. Soha, S. M. Spanier, A. Stahl, D. Su, M. K. Sullivan,
M. Talby, H. A. Tanaka, J. Va'vra, S. R. Wagner, A. J. R. Weinstein, W. J. Wisniewski, C. C. Young

Stanford Linear Accelerator Center, Stanford, CA 94309, USA

P. R. Burchat, C. H. Cheng, D. Kirkby, T. I. Meyer, C. Roat

Stanford University, Stanford, CA 94305-4060, USA

A. De Silva, R. Henderson

TRIUMF, Vancouver, BC, Canada V6T 2A3

W. Bugg, H. Cohn, E. Hart, A. W. Weidemann

University of Tennessee, Knoxville, TN 37996, USA

T. Benninger, J. M. Izen, I. Kitayama, X. C. Lou, M. Turcotte

University of Texas at Dallas, Richardson, TX 75083, USA

F. Bianchi, M. Bona, B. Di Girolamo, D. Gamba, A. Smol, D. Zanin

Università di Torino, Dipartimento di Fisica Sperimentale and INFN, I-10125 Torino, Italy

L. Bosisio, G. Della Ricca, L. Lanceri, A. Pompili, P. Poropat, M. Prest, E. Vallazza, G. Vuagnin

Università di Trieste, Dipartimento di Fisica and INFN, I-34127 Trieste, Italy

R. S. Panvini

Vanderbilt University, Nashville, TN 37235, USA

C. M. Brown, P. D. Jackson, R. Kowalewski, J. M. Roney

University of Victoria, Victoria, BC, Canada V8W 3P6

H. R. Band, E. Charles, S. Dasu, P. Elmer, J. R. Johnson, J. Nielsen, W. Orejudos, Y. Pan, R. Prepost,
I. J. Scott, J. Walsh, S. L. Wu, Z. Yu, H. Zobernig

University of Wisconsin, Madison, WI 53706, USA

1   Introduction

Measurements of the branching fractions for the rare charmless decays $B^0 \rightarrow h^+ h^-$ $(h = \pi, K)$[1] provide important information in the study of charge-parity (CP) violation. In principle, the $\pi^+ \pi^-$ decay mode can be used to extract the angle α of the Unitarity Triangle through the phenomenon of B^0-$\overline{B}^0$ mixing. However, in addition to the dominant $b \rightarrow uW^-$ tree amplitude, this decay includes the $b \rightarrow dg$ penguin amplitude and the determination of α is subject to large theoretical uncertainties if the penguin contribution is non-negligible [1]. In the presence of significant "penguin pollution," additional measurements of the isospin-related decays $B^- \rightarrow \pi^- \pi^0$ and $B \rightarrow \pi^0 \pi^0$ provide a means of measuring α cleanly in the $\pi\pi$ channel [2].

The decay $B^0 \rightarrow K^+ \pi^-$ is dominated by the $b \rightarrow sg$ penguin amplitude and provides an estimate of the scale of penguin pollution in the $\pi^+ \pi^-$ decay. Recent results from the CLEO collaboration indicate that the decay rate for $B^0 \rightarrow K^+ \pi^-$ is significantly larger than the rate for $B^0 \rightarrow \pi^+ \pi^-$ [3], implying that the penguin contribution in the $\pi\pi$ decay is indeed significant and an isospin analysis will be necessary to measure α accurately. The apparent enhancement of the penguin amplitude improves the prospects for observing direct CP violation as an asymmetry in the decay rates for $B^0 \rightarrow K^+ \pi^-$ and $\overline{B}^0 \rightarrow K^- \pi^+$. Precise measurement of the decay rates for $\pi\pi$ and $K\pi$ decays is therefore of central importance. This paper describes preliminary measurements of branching fractions for the decays $B^0 \rightarrow \pi^+ \pi^-$, $K^+ \pi^-$, and $K^+ K^-$ with the first data collected by the *BABAR* experiment.

2   Data sample, *BABAR* detector, and event selection

The dataset used in this analysis consists of $8.9 \, \mathrm{fb}^{-1}$ collected with the *BABAR* detector at the Stanford Linear Accelerator Center's PEP-II storage ring between January and June 2000. The PEP-II facility operates nominally at the $\Upsilon(4S)$ resonance, providing asymmetric collisions of 9.0 GeV electrons on 3.1 GeV positrons. The dataset includes $7.7 \, \mathrm{fb}^{-1}$ collected in this configuration (on-resonance) and $1.2 \, \mathrm{fb}^{-1}$ collected below the $B\overline{B}$ threshold (off-resonance) that are used for continuum background studies. The on-resonance sample corresponds to 8.8 million produced $B\overline{B}$ events.

The asymmetric beam configuration in the laboratory frame provides a boost ($\beta\gamma = 0.56$) to the $\Upsilon(4S)$, allowing separation of the B and $\overline{B}$ decay products for time-dependent CP-violation studies. For the analysis described in this paper, the significant effect of the boost relative to symmetric collider experiments is to increase the momentum range of the B decay products from a narrow distribution centered at $\sim 2.6 \, \mathrm{GeV}/c$, to a broad distribution extending from 1.5 to $4.5 \, \mathrm{GeV}/c$. Wherever necessary, kinematic quantities evaluated in the $\Upsilon(4S)$ center-of-mass (CM) frame are denoted with an additional superscript asterisk in order to distinguish them from the corresponding quantities evaluated in the laboratory frame.

BABAR is a solenoidal detector optimized for the asymmetric beam configuration at PEP-II and is described in detail elsewhere [4]. Charged particle (track) momenta are measured in a tracking system consisting of a 5-layer, double-sided, silicon vertex tracker and a 40-layer drift chamber filled with a gas mixture of helium and isobutane, both operating within a 1.5 T superconducting solenoidal magnet. Photons are detected in an electromagnetic calorimeter consisting of 6580 CsI(Tl) crystals arranged in barrel and forward endcap subdetectors that also operates within the magnetic field. The iron used for the magnet yoke is segmented and instrumented with resistive

---

[1]Charge conjugate decay modes are assumed throughout this paper.

plate chambers, providing muon identification and (in conjunction with the calorimeter) neutral hadron detection.

In this analysis, tracks are identified as pions or kaons by the Čerenkov angle θ_c measured by a Detector of Internally Reflected Čerenkov light (DIRC). The DIRC system is a unique type of Čerenkov detector that relies on total internal reflection within the radiator to deliver the Čerenkov light outside the tracking and magnetic volumes. The radiator consists of 144 axially aligned synthetic quartz bars located just inside the inner radius of the calorimeter. The bars extend outside the solenoid flux return in the backward direction, where the Čerenkov ring is imaged by an array of ~ 11000 photomultiplier tubes.

Hadronic events are selected based on track multiplicity and event topology. Tracks with transverse momentum greater than $100\,\mathrm{MeV}/c$ are required to pass efficient quality cuts, including number of drift chamber hit layers used in the track fit and impact parameter in the r–ϕ and r–z planes, where the cylindrical coordinate z is aligned along the detector axis in the electron beam direction. At least three tracks must pass the above selection. To reduce contamination from Bhabha and $\mu^+\mu^-$ events the ratio of second to zeroth Fox-Wolfram moments [5], $R_2 = H_2/H_0$, is required to be less than 0.95. Residual background from tau hadronic decays is reduced by requiring the sphericity [6] of the event to be greater than 0.01. The efficiency of the event selection is dominated by the acceptance and efficiency of the track requirement, and is determined to be 70% from a detailed Monte Carlo simulation based on `Geant321` [7].

3   Selection of $B \to h^+h^-$ candidates

One of the advantages of measuring B decay parameters at the $\Upsilon(4S)$ resonance is the kinematic constraint provided by the initial state, where energy conservation determines that the energies of the B mesons in the CM frame are equal to $\sqrt{s}/2$, where $\sqrt{s}$ is the total e^+e^- CM energy. We exploit this constraint by calculating an energy-substituted mass m_{ES}, where $\sqrt{s}/2$ is substituted for the B candidate energy, and by calculating the energy difference ΔE between the B candidate and $\sqrt{s}/2$ in the CM frame.

We define $m_{\mathrm{ES}} = \sqrt{(\sqrt{s}/2)^2 - p_B^{*2}}$, where p_B^* is the B candidate momentum evaluated in the CM frame. Because p_B^* is relatively small ($\sim 300\,\mathrm{MeV}/c$), the resolution on m_{ES} is dominated by the uncertainty in $\sqrt{s}$, which in turn is determined by the beam energy spread and width of the $\Upsilon(4S)$ resonance. Substitution of the beam energy reduces the mass resolution by one order of magnitude compared to the invariant mass. The mean value of m_{ES} and its Gaussian width $\sigma(m_{\mathrm{ES}})$ are determined from a large sample of fully reconstructed B decays. We find $m_{\mathrm{ES}} = (5.2800 \pm 0.0005)\,\mathrm{GeV}/c^2$ and $\sigma(m_{\mathrm{ES}}) = (2.6 \pm 0.1)\,\mathrm{MeV}/c^2$, respectively. Our initial selection requires $5.22 < m_{\mathrm{ES}} < 5.30\,\mathrm{GeV}/c^2$.

We define $\Delta E = E_B^* - \sqrt{s}/2$, where E_B^* is the B candidate energy in the CM frame. Signal events are Gaussianly distributed in ΔE with a mean near zero, while the continuum background falls linearly over the region of interest. For this analysis, the pion mass is assigned to all tracks and the $K\pi$ and KK decays have ΔE shifted from zero by an amount depending on the momentum of the tracks. From Monte Carlo simulation we find shifts of -45 and $-91\,\mathrm{MeV}$ for the $K\pi$ and KK decays, respectively. The resolution on ΔE is estimated to be $27 \pm 5\,\mathrm{MeV}$ based on Monte Carlo simulated $\pi\pi$ decays and the observed difference in widths between data and Monte Carlo $B^- \to D^0\pi^-$ decays. We require $|\Delta E| < 0.420\,\mathrm{GeV}$.

4 Background suppression

Due to the relatively small CM momenta of decay products produced from the quark transition $b \to c$, B decays to final states involving charm mesons are not a significant background to charmless two-body decays. After hadronic selection, the background is dominated by continuum production of light quarks, $e^+e^- \to q\overline{q}\,(q = u, d, s, c)$. In the CM frame, the continuum background typically exhibits a two-jet structure that can produce two high momentum back-to-back tracks with an invariant mass near the B mass. In contrast, the low momentum of B mesons in the decay $\Upsilon(4S) \to B\overline{B}$ leads to a more spherically symmetric event. This topology difference is exploited by constructing the angle θ_S between the sphericity axes, evaluated in the CM frame, of the B candidate and the remaining charged and neutral particles in the event. The absolute value of the cosine of this angle is strongly peaked near 1 for continuum events and is approximately uniform for $B\overline{B}$ events. We require $|\cos\theta_S| < 0.9$, which is 87% efficient for signal events and rejects 66% of the continuum background.

Further separation power between signal and continuum background is provided by a Fisher discriminant technique [8]. The Fisher discriminant $\mathcal{F}$ is calculated from a linear combination of discriminating variables x_i,

$$\mathcal{F} = \sum_{i=1}^{9} \alpha_i x_i, \tag{1}$$

where the coefficients α_i are chosen to maximize the statistical separation between signal and background events. The nine discriminating variables are constructed from the scalar sum of the momenta of all charged and neutral particles (excluding the candidate daughter tracks) flowing into nine concentric cones centered on the B-candidate thrust axis in the CM frame. Each cone subtends an angle of $10°$ and is folded to combine the forward and backward intervals. More energy will be found in the cones nearer the candidate thrust axis in jet-like continuum background events than in the more isotropic $B\overline{B}$ events.

Large samples of signal and background Monte Carlo simulated events reconstructed in the $\pi\pi$ mode are used to determine the Fisher coefficients. Figure 1 shows the resulting $\mathcal{F}$ distributions for signal $\pi\pi$ Monte Carlo compared to a sample of $B^- \to D^0\pi^-$ decays reconstructed in data, and continuum background Monte Carlo compared to off-resonance data. The $\mathcal{F}$ distributions for both signal and background are parameterized by the sum of two Gaussians with separate means and widths. The Gaussian fits are performed on Monte Carlo samples that are independent of the samples used to determine the Fisher coefficients, and the same parameterization is used for all three signal modes.

5 Particle identification

Two complementary methods of exploiting the particle identification capabilities of the DIRC are described in this paper. The first method uses measurements of θ_c to derive particle *selectors* that are used to identify pions and kaons on a per-track basis. The second method uses likelihood functions derived from θ_c measurements directly in a maximum-likelihood fit to extract the relative amount of each decay mode on a statistical basis. After the selection criteria described above, the combined acceptance and efficiency of requiring a θ_c measurement for both tracks is 76%.

A control sample consisting of 18141 ± 140 $D^0 \to K^-\pi^+$ candidate decays is used to parameterize and assess the performance of both particle identification methods. A 96% pure D^0 sample
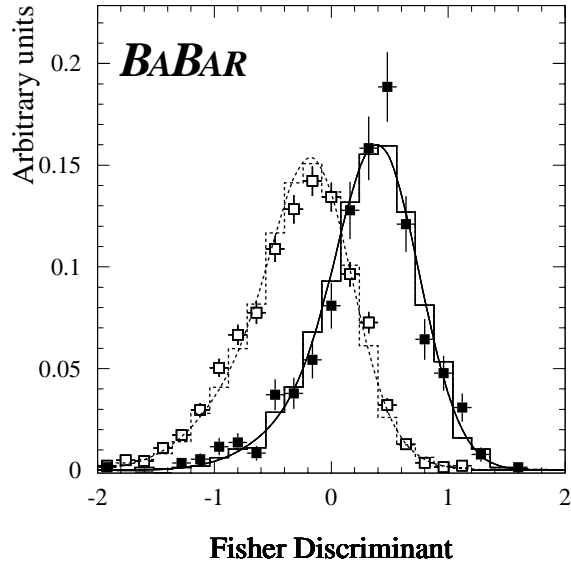
Figure 1: The $\mathcal{F}$ distribution for $\pi\pi$ signal Monte Carlo events (solid histogram and fitted curve) compared to data $B^- \to D^0\pi^-$ decays (filled squares), and continuum background Monte Carlo (dashed histogram and fitted curve) compared to off-resonance data (open squares). The Monte Carlo samples are independent of the samples used to train the Fisher discriminant.

is obtained through the decay $D^{*+} \to D^0\pi_s^+$, where the slow pion π_s^+ tags the charge of the pion from the D^0 decay. Requiring a tight window around the D^{*+}–D^0 mass difference minimizes contamination from incorrectly reconstructed D^0 mesons, where the two daughter tracks are assigned the incorrect particle hypotheses. The momentum of kaons and pions in the control sample ranges from 1.75–4.0 GeV/c, which covers 90% of the momentum range for charmless two-body B decays.

The performance of the DIRC is summarized in Fig. 2, where we show plots of (a) θ_c vs. p for tracks in the control sample and (b) the statistical separation between pions and kaons as a function of momentum. The separation, defined as $\left[\langle\theta_c(\pi)\rangle - \langle\theta_c(K)\rangle\right]/\langle\sigma_{\theta_c}\rangle$, where $\langle\theta_c(h)\rangle$ are the Gaussian means for pion and kaon tracks and $\langle\sigma_{\theta_c}\rangle$ is the average width, varies from 8 at 2 GeV/c to 2.5 at 4 GeV/c. Note that the quoted θ_c separation is for a single track and an average over the polar angle of each track is implicit in Fig. 2(b).

The selector method of particle identification attempts to identify pions and kaons on a per-track basis by cutting on likelihood functions. We construct the likelihood for a given mass hypothesis from the Gaussianly-distributed θ_c measurements and the Poissonian probability for the number of measured Čerenkov photons compared to its expectation value. Tracks with momentum below the kaon threshold or within $2\sigma(\theta_c)$ of the expected value for a proton are explicitly removed, where the measurement error $\sigma(\theta_c)$ varies with momentum and the number of photons used in the fit. We calculate the efficiency for one mode to be identified as another using the efficiency and mis-identification probabilities for pions and kaons measured in the D^0 control sample. The resulting efficiency matrix is shown in Table 1. The matrix includes the probability that a pion or kaon is mis-measured and removed by the proton rejection requirement.

The global likelihood method incorporates the particle identification probabilities for pions
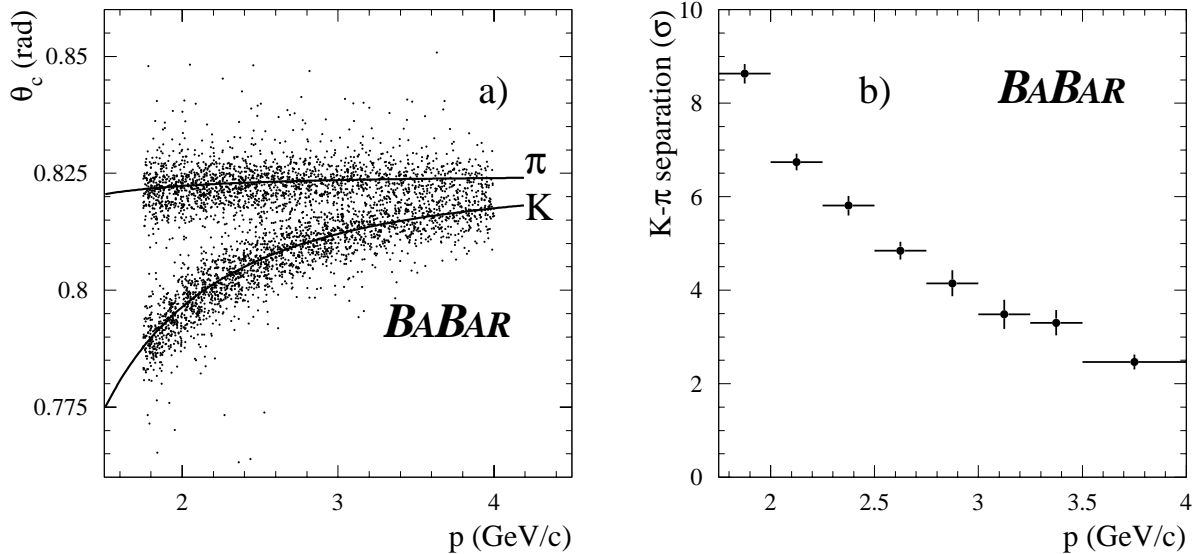
11

Figure 2: (a) The Čerenkov angle and (b) K–π separation as functions of momentum for single tracks in the D^0 control sample. The separation is an average over all polar angles.

Table 1: Particle selector efficiency and mis-identification probability for each decay mode. Errors are statistical only.

	Probability to be identified as		
Mode	$\pi\pi$	$K\pi$	KK
$\pi\pi$	0.853 ± 0.005	0.109 ± 0.008	0.0029 ± 0.0002
$K\pi$	0.121 ± 0.004	0.775 ± 0.006	0.051 ± 0.004
KK	0.0112 ± 0.0006	0.231 ± 0.008	0.704 ± 0.007

and kaons directly in an unbinned maximum likelihood fit. The probability density functions are constructed from θ_c information alone, where Gaussian fits are performed to the distribution of measured $-$ expected Čerenkov angle in bins of momentum in the D^0 control sample. To improve the resolution and minimize the non-Gaussian tails of the θ_c distribution, we require a minimum number of observed Čerenkov photons above the expected background. From the control sample we determine the efficiency of this requirement to be 77%, taking into account the angular correlation between the two daughter tracks from a B decay. The proton rejection cut applied in the selector method is also required for the likelihood analysis. After the minimum photon cut, the proton requirement is 98% efficient for h^+h^- events.

6   Analysis

In this section we present the results of a simple cut-based analysis to determine the h^+h^- yield, followed by two complementary methods for determining the $\pi\pi$, $K\pi$, and KK yields in our data.

12

In the first method we apply background suppression and particle identification cuts to isolate samples of events that are consistent with the $\pi\pi$, $K\pi$, or KK hypotheses. Signal yields are then obtained from an unbinned maximum likelihood fit to m_{ES}. In the second method we perform a global maximum likelihood fit incorporating m_{ES}, ΔE, and $\mathcal{F}$, as well as the θ_c probability density functions described in the previous section, to determine signal yields in all three modes simultaneously. The cut-based method is more transparent while the global fit has higher efficiency and statistical significance. In Sec. 7 we calculate branching fractions using the global fit results.

6.1 Cut-based analysis

In addition to the selection criteria described in Secs. 3 and 4, we tighten the θ_S requirement, $|\cos\theta_S| < 0.7$, and also require $|\cos\theta_B| < 0.8$, where θ_B is the CM angle of the B candidate with respect to the beam. The variable $\cos\theta_B$ is uniform for the continuum background and follows a $1 - \cos^2\theta_B$ distribution for signal B decays. We determine an optimal selection requirement of $\mathcal{F} > 0.37$ by maximizing the statistical significance of the expected signal yield in a sample of Monte Carlo simulated signal and background events. The relative efficiency of these additional cuts is 44%. Within the ΔE–m_{ES} plane we define a signal region $|\Delta E| < 0.140\,\mathrm{GeV}$ and $m_{\mathrm{ES}} = 5.2800 \pm 0.0052\,\mathrm{GeV}/c^2$, and sideband regions $|\Delta E| > 0.140\,\mathrm{GeV}$ and $m_{\mathrm{ES}} < 5.27\,\mathrm{GeV}/c^2$. The signal region in ΔE is designed to minimize contamination from three-body charmless B decays where one of the decay products has low momentum.

Before applying the particle selector we first demonstrate the presence of h^+h^- decays in the signal region. The signal yield is obtained from an unbinned maximum likelihood fit to the m_{ES} distribution. The fit includes candidates passing all cuts except the requirement that the tracks have an associated θ_c measurement. The background shape in m_{ES} is parameterized by the empirical formula [9],

$$f(m_{\mathrm{ES}}) \propto m_{\mathrm{ES}} \sqrt{1 - x^2} \exp\left[-\xi(1 - x^2)\right], \tag{2}$$

where $x = 2m_{\mathrm{ES}}/\sqrt{s}$ and the parameter ξ is determined from a fit. Figure 3 shows the results of fitting Eq. 2 to the on-resonance ΔE sideband region, where we find $\xi = 22.0 \pm 0.5$. We then fit the m_{ES} distribution in the ΔE signal region to a Gaussian with mean and width fixed to $5.280\,\mathrm{GeV}/c^2$ and $2.6\,\mathrm{MeV}/c^2$, respectively, and the background shape fixed to $\xi = 22$; only the normalizations are free parameters. The result is shown in Fig. 4. The fitted number of h^+h^- candidates is 67 ± 11, where the error is the statistical uncertainty from the fit. Correcting for the total efficiency of the selection criteria (27%) and normalizing to the total number of $B\overline{B}$ pairs, we determine a branching fraction $\mathcal{B}(B^0 \to h^+h^-) = (28 \pm 5) \times 10^{-6}$, where the error is statistical only and we assume equal $\Upsilon(4S)$ branching fractions to charged and neutral B mesons.

The presence of kaons in the signal region can be demonstrated by plotting the variable $(\theta_c - \theta_c(\pi))/(\theta_c(\pi) - \theta_c(K))$, where $\theta_c(\pi)$ and $\theta_c(K)$ are the expected values. This variable peaks at $0\,(-1)$ for real pion (kaon) tracks. In Fig. 5 we show the distribution of this variable for B-candidate tracks in the m_{ES} signal region before and after subtracting the distribution obtained from the m_{ES} sideband region. A clear kaon peak remains after subtraction.

We now decompose the signal into its constituent components by using the particle selector to separate the sample into three subsamples corresponding to the different channels. We perform three separate fits similar to the h^+h^- fit. After correcting for the efficiency and mis-identification probabilities in Table 1, we find 25 ± 8 $\pi\pi$, 26 ± 8 $K\pi$, and $1.2^{+3.8}_{-1.2}$ KK decays. In Fig. 6 we show the fit results for m_{ES} and the ΔE distribution in the m_{ES} signal region for all three modes.
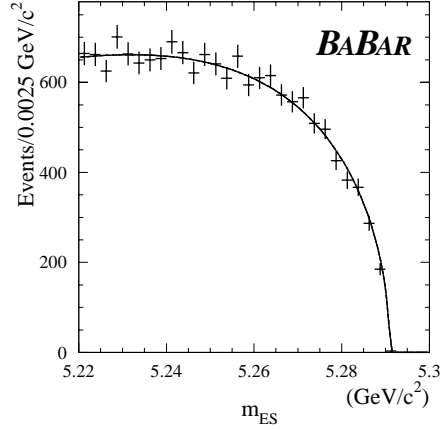
Figure 3: Result of fitting of Eq. 2 to the ΔE sideband region in on-resonance data. The result is $\xi = 22.0 \pm 0.5$.
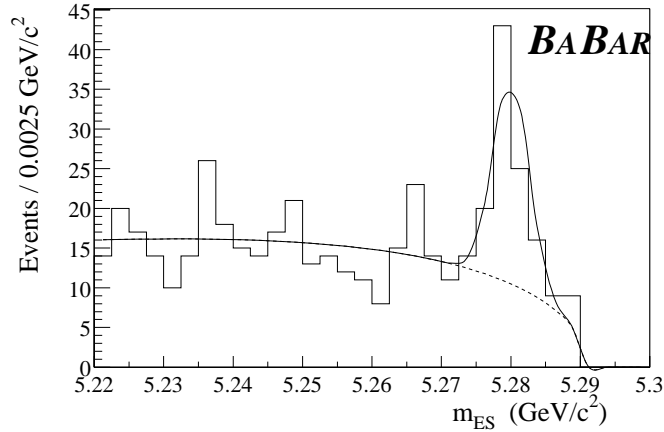

Figure 4: Result of fitting the m_{ES} signal region in the h^+h^- sample to the sum of Eq. 2, with $\xi = 22$, and a Gaussian signal peak with $m_{\mathrm{ES}} = 5.28\,\mathrm{GeV}/c^2$ and $\sigma(m_{\mathrm{ES}}) = 2.6\,\mathrm{MeV}/c^2$. The dashed curve shows the background parameterization only.

To facilitate comparison with the global maximum likelihood fit, we determine the non-common systematic errors for the cut-based analysis. We vary the mean and width of the m_{ES} signal and background distributions within their estimated uncertainties. Systematic uncertainty on the particle identification method is estimated by comparing with various selector definitions, including the probability density functions used in the global fit (below). Uncertainty in the $\mathcal{F}$ shape is estimated by varying the cut and by substituting the shape obtained from the $B^- \to D^0\pi^-$ data sample (Fig. 1). Table 2 summarizes these uncertainties.
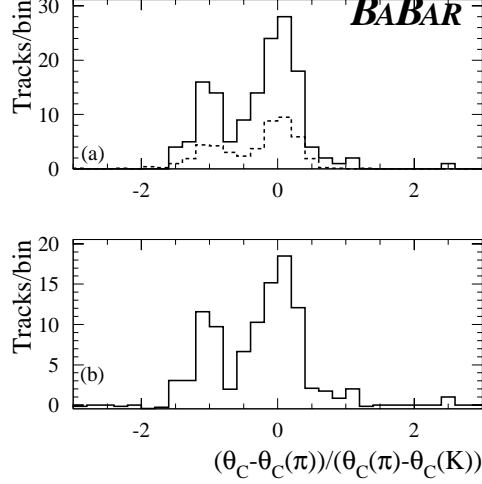
Figure 5: The measured Čerenkov angle minus its expectation value for the pion hypothesis, normalized to the expected separation between pions and kaons. True pions (kaons) appear as a peak at $0\,(-1)$. (a) shows the distribution for B candidate tracks in the signal region of ΔE and the signal (solid) and sideband (dashed) regions of m_{ES}, while (b) shows the signal region after sideband subtraction. Note that both tracks from each B candidate are included in these plots.
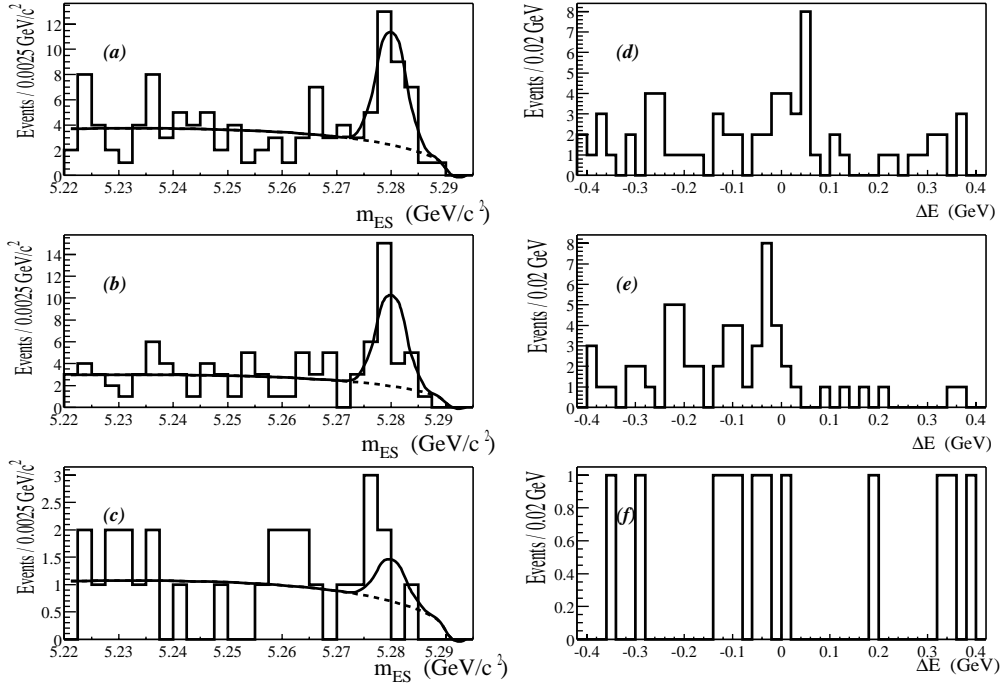
Figure 6: Fit results for m_{ES} in the (a) $\pi\pi$, (b) $K\pi$, and (c) KK samples defined by the particle identification selector described in Sec. 5. Also shown are the ΔE distributions for the (d) $\pi\pi$, (e) $K\pi$, and (f) KK samples in the m_{ES} signal region.

15

Table 2: Systematic errors (%) in the cut-based analysis that are not common to the global fit analysis. "PID" refers to the method of particle identification.

Mode	Bkg m_{ES}	$\langle m_{\mathrm{ES}} \rangle$	$\sigma(m_{\mathrm{ES}})$	$\mathcal{F}(D^0\pi)$	$\mathcal{F}$ cut	PID	Total
$\pi^+\pi^-$	0.4	$+0.4$ -1.2	0.8	1.9	11	9	± 14
$K^+\pi^-$	0.4	$+1.7$ -3.0	0.8	1.9	8	9	± 13
K^+K^-	0.5	$+23$ -27	$+2.7$ -5.3	1.9	14	14	$+31$ -34
h^+h^-	0.5	$+1.2$ -2.7	$+1.3$ -1.2	1.9	6	–	7

6.2 Global fit

We perform an unbinned maximum likelihood fit using m_{ES}, ΔE, $\mathcal{F}$, $\theta_1(p_1)$, and $\theta_2(p_2)$, where θ_1 and θ_2 are the Čerenkov angles for each track and p_1 and p_2 are the momenta. The likelihood $\mathcal{L}$ is defined as

$$\mathcal{L} = e^{-N'} \prod_{i=1}^{N} \mathcal{P}_i(m_{\mathrm{ES}}, \Delta E, \mathcal{F}, \theta_1(p_1), \theta_2(p_2) | N_{\pi\pi}, N_{K\pi}, N_{\pi K}, N_{KK}, N_{\mathrm{bkg}}), \tag{3}$$

where N_{bkg} is the number of continuum background events and $\mathcal{P}_i$ is the probability for the ith candidate assuming the total yield

$$N' = N_{\pi\pi} + N_{K\pi} + N_{\pi K} + N_{KK} + N_{\mathrm{bkg}}. \tag{4}$$

In the $K\pi$ mode we fit separately for the two possible combinations (πK or $K\pi$). The term $(e^{-N'})$ derives from the Poissonian probability of observing N total events when N' are expected. The probability for a given candidate is the sum of the signal and background terms

$$\mathcal{P}_i(m_{\mathrm{ES}}, \Delta E, \mathcal{F}, \theta_1(p_1), \theta_2(p_2) | N_{\pi\pi}, N_{K\pi}, N_{\pi K}, N_{KK}, N_{\mathrm{bkg}}) = \sum_k N_k \mathcal{P}_i^k, \tag{5}$$

where the index k represents the five fit components and $\mathcal{P}_i^k$ is the product of probability density functions for m_{ES}, ΔE, $\mathcal{F}$, $\theta_1(p_1)$, and $\theta_2(p_2)$.

The fit includes all candidates satisfying the selection criteria described in Secs. 2, 3, and 4, as well as the requirement on the number of Čerenkov photons above background and the proton rejection cut described in Sec. 5. Due to the use of the discriminating variable ΔE, the global fit is much less susceptible to contamination from three-body B decays. The signal region is therefore expanded to $-0.200 < \Delta E < 0.140\,\mathrm{GeV}$. The quantity $-\log \mathcal{L}$ is minimized with respect to the fit parameters. The resulting signal yields are 29^{+8}_{-7} $\pi\pi$, 38^{+9}_{-8} $K\pi$, and 7^{+5}_{-4} KK decays. As a visual cross check, in Fig. 7 we plot the m_{ES}, ΔE, and θ_c distributions after the additional requirements on $\cos\theta_S$, $\cos\theta_B$, and $\mathcal{F}$ applied in the cut-based analysis, and overlay the global fit results after rescaling by the relative efficiency for these cuts.

Systematic errors on the fit results are estimated by varying the signal and background probability density functions for m_{ES}, ΔE, and θ_c within their errors. The ΔE width is significantly different between data and Monte Carlo simulated $B^- \to D^0\pi^-$ decays and there is evidence for a few MeV shift of the mean value in the negative direction. To be conservative we vary the width by
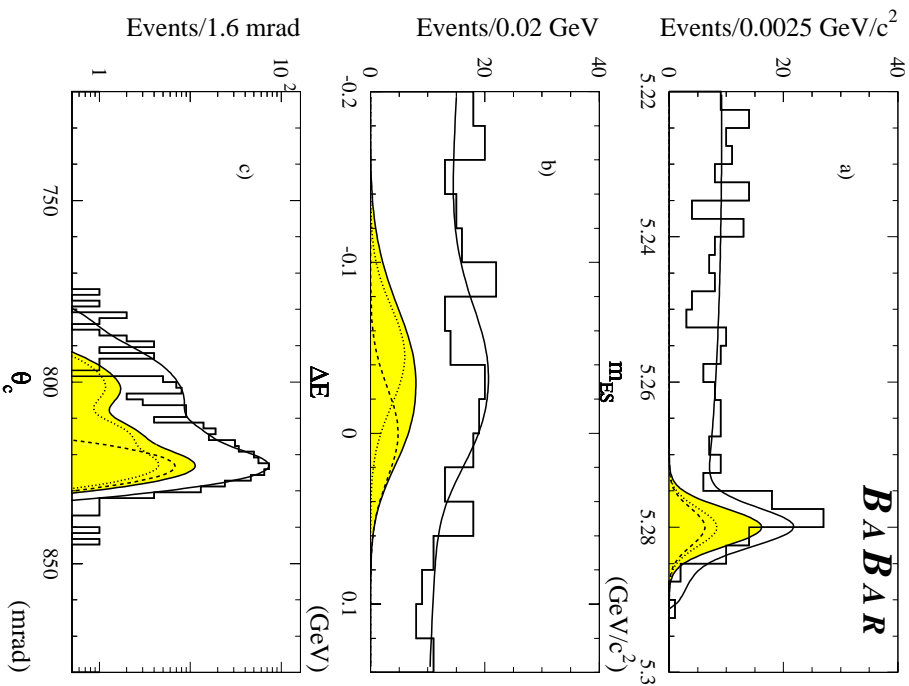
Figure 7: The distributions of (a) m_{ES}, (b) ΔE, and (c) θ_c (solid histograms) after cutting on $\cos\theta_S$, $\cos\theta_B$, and $\mathcal{F}$. The global fit results are overlaid after scaling by the relative efficiency of the additional cuts. The shaded region is the total signal contribution, while the dashed and dotted lines are the $\pi\pi$ and $K\pi$ components, respectively.

Table 3: Systematic errors (%) on the signal yield from the global fit that are not common to the cut-based analysis. Uncertainty on θ_c includes mean and width.

Mode	Bkg m_{ES}	Bkg ΔE	$\langle m_{ES}\rangle$	$\sigma(m_{ES})$	$\langle\Delta E\rangle$	$\sigma(\Delta E)$	$\mathcal{F}(D^0\pi)$	θ_c	Total
$\pi^+\pi^-$	0.2	0.4	$+0.7$ -2.0	0.3	$+1.9$	$+7$ -10	7.0	$+3.5$ -2.4	$+11$ -13
$K^+\pi^-$	0.2	0.2	$+1.0$ -5	$+0.3$ -0.4	-0.7	$+5$ -9	5	$+1.0$ -1.4	$+7$ -12
K^+K^-	0.3	6	$+1.3$ -3.1	$+2.1$ -2.5	-3.1	$+2.7$ -2.9	22	2.0	$+23$ -24

$\pm 5\,\mathrm{MeV}$ and refit assuming $\langle \Delta E \rangle = -5\,\mathrm{MeV}$. The uncertainty due to the shape of $\mathcal{F}$ is determined by using the shape obtained from data $B^- \to D^0 \pi^-$ decays. Table 3 summarizes the systematic errors that are not common to the cut-based analysis.

6.3 Comparison and cross-checks

In order to compare results for the two methods, we correct the signal yields obtained in the cut-based analysis by the relative efficiency of the $|\cos\theta_S| < 0.7$, $|\cos\theta_B| < 0.8$, and $\mathcal{F} > 0.37$ cuts (44%), and the global likelihood fit yields by the efficiency of the Čerenkov photon cut and proton rejection cuts (76%). In order to compare total yields to the h^+h^- fit result we also correct by the common requirement that both tracks have an associated θ_c measurement (76%). The resulting comparison is summarized in Table 4. Given that the two samples are not 100% statistically correlated, we find the agreement to be satisfactory.

As a cross-check we perform the global fit after applying the particle selector and the additional selection criteria used in the cut-based analysis (including $|\Delta E| < 0.140\,\mathrm{GeV}$). The ΔE and θ_c distributions are used in the fit, the $\mathcal{F}$ distribution is not. The results, summarized in Table 5, indicate that there is no significant migration between signal categories. This result confirms the consistency in the use of θ_c in both analyses.

Table 4: Comparison of signal yields corrected for the relative efficiency of cut-based and global fit analyses. The first uncertainty is statistical, the second is systematic. For total h^+h^- yield we compare the sum of central values for the individual modes in the two analyses with the h^+h^- fit result (Fig. 4).

Mode	cut-based	global fit	h^+h^- fit
$\pi^+\pi^-$	$76 \pm 23 \pm 11$	$50^{+14\,+6}_{-12\,-7}$	–
$K^+\pi^-$	$77 \pm 25 \pm 10$	$67^{+16\,+5}_{-14\,-8}$	–
K^+K^-	$4^{+11}_{-4}\pm 1$	$13^{+9}_{-7}\pm 3$	–
h^+h^-	156	129	$151 \pm 24 \pm 11$

Table 5: Signal yields from global fits to the particle-selected samples. Note that these results have not been corrected for the 76% efficiency of the cut on minimum number of Čerenkov photons.

	Selected as		
Mode	$\pi\pi$	$K\pi$	KK
$\pi\pi$	21 ± 5	$0.0^{+0.7}_{-0.0}$	$0.0^{+0.5}_{-0.0}$
$K\pi$	$0.0^{+0.7}_{-0.0}$	24 ± 5	$0.0^{+0.7}_{-0.0}$
KK	$0.0^{+0.5}_{-0.0}$	1.7 ± 2.3	2.1 ± 1.9

Table 6: Summary of branching fraction results for the global likelihood fit. Shown are the central fit values N_S, the statistical significance, and the measured branching fractions $\mathcal{B}$. For the KK mode, the 90% confidence level upper limit on the signal yield is given in parenthesis. There is a common efficiency of 0.35 ± 0.02 for all three modes. For N_S and $\mathcal{B}$ the first error is statistical and the second is systematic. Charge conjugate modes are assumed.

Mode	N_S	Stat. Sig. (σ)	$\mathcal{B}\,(10^{-6})$
$\pi^+\pi^-$	29^{+8+3}_{-7-4}	5.7	$9.3^{+2.6+1.2}_{-2.3-1.4}$
$K^+\pi^-$	38^{+9+3}_{-8-5}	6.7	$12.5^{+3.0+1.3}_{-2.6-1.7}$
K^+K^-	$7^{+5}_{-4}\;(<15)$	2.1	<6.6

7 Determination of branching fractions

We determine branching fractions for $\pi^+\pi^-$ and $K^+\pi^-$ decays and an upper limit for the K^+K^- decay using the results of the global likelihood fit. The individual efficiencies were reported in previous sections. The total efficiency is 0.35 ± 0.02, where the error is combined statistical and systematic. Branching fractions are calculated as

$$\mathcal{B} = \frac{N_S}{\epsilon \cdot N_{B\overline{B}}},\qquad(6)$$

where N_S is the central value from the fit, ϵ is the total efficiency, and $N_{B\overline{B}}$ is the total number of $B\overline{B}$ pairs in our dataset. Implicit in Eq. 6 is the assumption of equal branching fractions for $\Upsilon(4S) \to B^0\overline{B}^0$ and $\Upsilon(4S) \to B^+B^-$. The results are summarized in Table 6. In addition to the systematic uncertainties listed in Table 3, the total error includes uncertainty on the tracking efficiency (2.5% per track) [4], the shape of $\cos\theta_S$ (3%), and the number of $B\overline{B}$ events (3.6%).

The statistical significance of a given signal yield is determined by setting the yield to zero and maximizing the likelihood with respect to the remaining variables. The results are give in Table 6. Fig. 8 shows the $n\sigma$ likelihood contour curves, where σ represents the statistical uncertainty only. The curves are computed by maximizing the likelihood with respect to the remaining variables in the fit. For the KK mode we calculate the 90% confidence level upper limit yield and decrease the efficiency by the total systematic error (24%) before calculating the upper limit branching fraction.

8 Summary

We have performed a search for charmless two-body B decays to charged pions and kaons. The statistical significance of the signal yields are 5.7, 6.7, and 2.1 standard deviations for the $\pi\pi$, $K\pi$, and KK decay modes, respectively. For the decay modes $B^0 \to \pi^+\pi^-$ and $B^0 \to K^+\pi^-$ we measure preliminary branching fractions of $(9.3^{+2.6+1.2}_{-2.3-1.4}) \times 10^{-6}$ and $(12.5^{+3.0+1.3}_{-2.6-1.7}) \times 10^{-6}$, respectively, where the first uncertainty is statistical and the second is systematic. Since the KK yield is not significant we calculate the 90% confidence limit and find $\mathcal{B}(B^0 \to K^+K^-) < 6.6 \times 10^{-6}$.
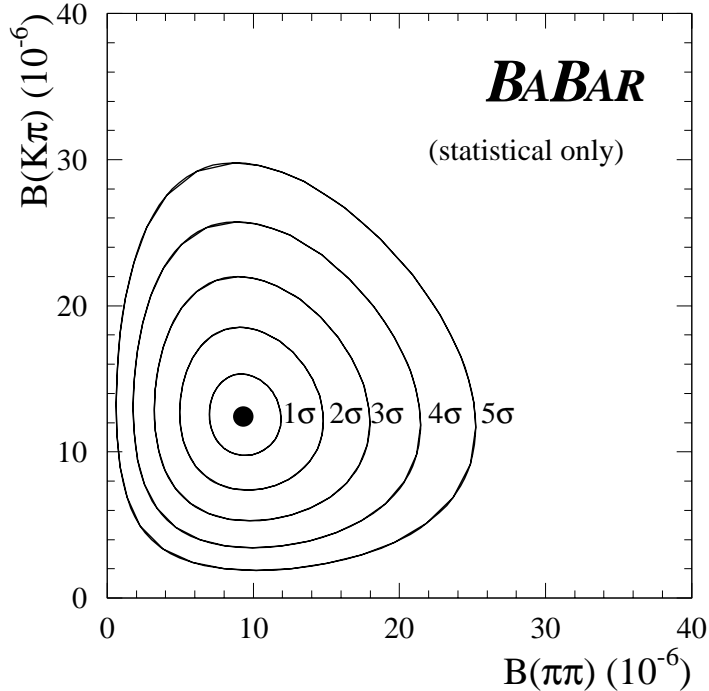
Figure 8: The central value (filled circle) for $\mathcal{B}(B^0 \to \pi^+\pi^-)$ and $\mathcal{B}(B^0 \to K^+\pi^-)$ along with the $n\sigma$ statistical contour curves for the global likelihood fit, where $n\sigma$ corresponds to a change of n^2 in $-2\log\mathcal{L}$.

Acknowledgments

References

[1] M. Gronau, Phys. Rev. Lett. **63**, 1451 (1989).

[2] M. Gronau, Phys. Rev. Lett. **65**, 3381 (1990).

[3] CLEO Collaboration, D. Cronin-Hennessy *et al.*, Phys. Rev. Lett. **85**, 515 (2000).

[4] *BABAR* Collaboration, B. Aubert *et al.*, "The first year of the *BABAR* experiment at PEP-II", *BABAR*-CONF-00/17, submitted to the XXXth International Conference on High Energy Physics, Osaka, Japan.

[5] G. C. Fox and S. Wolfram, Nucl. Phys. **B149**, 413 (1979).

[6] S. L. Wu, Phys. Rep.**107**, 59 (1984).

[7] CERN Application Software Group, GEANT Version 3.21, CERN Program Library Long Writeup W5013, 1994.

[8] CLEO Collaboration, D. M. Asner *et al.*, Phys. Rev. **D53**, 1039 (1996).

[9] ARGUS Collaboration, H. Albrecht *et al.*, Z. Phys. C **48**, 543 (1990).